Acoustic and thermal transport properties of hard carbon formed from C_60 fullerene

Lasjaunias, J. C.; Saint-Paul, M.; Bilušić, A.; Smontara, Ana; Gradečak, S.; Tonejc, Anđelka; Tonejc, Antun; Kitamura, N.

Journal article, Published version
Rad u časopisu, Objavljena verzija rada (izdavačev PDF)

Acoustic and thermal transport properties of hard carbon formed from C_{60} fullerene

J. C. Lasjaunias* and M. Saint-Paul

Centre de Recherches sur les Très Basses Températures, laboratoire associé à l'Université Joseph Fourier, C.N.R.S., BP 166, 38042 Grenoble, France

A. Bilušić and A. Smontara

Institute of Physics, Bijenicka 46, P.O. Box 304, HR-10 001 Zagreb, Croatia

S. Gradečak

Centre Interdépartmental de Microscopie Electronique, École Polytechnique Fédérale de Lausanne, CH-1015 Lausanne, Switzerland

A. M. Tonejc and A. Tonejc

Department of Physics, Faculty of Sciences, University of Zagreb, Bijenicka 32, HR-10001 Zagreb, Croatia

N. Kitamura

Osaka National Research Laboratory, Ikeda, Osaka, 563, Japan

We report on extended investigation of the thermal transport and acoustical properties on hard carbon samples obtained by pressurization of C_{60} fullerene. Structural investigations performed by different techniques on the same samples indicate a very inhomogeneous structure at different scales, based on fractal-like amorphous clusters on the micrometer to submillimeter scale, which act as strong acoustic scatterers, and scarce microcrystallites on the nanometer scale. Ultrasonic experiments show a rapid increase in the attenuation with frequency, corresponding to a decrease in the localization length for vibrations. The data give evidence for a crossover from extended phonon excitations to localized fracton excitations. The thermal conductivity is characterized by a monotonous increase versus temperature, power law $T^{1.4}$, for T ranging from 0.1 to 10 K, without any well-defined plateau, and a strictly linear-in-T variation between 20 and 300 K. The latter has to be related to the linear-in-T decrease of the sound velocity between 4 and 100 K, both linear regimes being characteristic of disordered or generally aperiodic structures, which can be analyzed by the "phonon-fracton hopping" model developed for fractal and amorphous structures.

I. INTRODUCTION

Hard carbon (HC), obtained by high-temperature pressurization of initial fullerene C_{60}, is of great practical interest due to its high hardness, about 2/3 of that of diamond, and, at the same time, semimetallic electrical resistivity, very similar to graphite. However, until recently, only a few physical properties have been investigated in hard carbon, except for electrical resistivity, x-ray diffraction, Raman measurements,[1] and neutron structural investigations.[2] The first thermal transport measurements[3] were performed between 30 and 350 K on a hard carbon sample pressurised at 2.6–3 GPa and a temperature of 973 K.[1] The main result is that the thermal conductivity varies linearly with temperature in the whole temperature range investigated. Very recently, thermal conductivity was measured down to 4 K on C_{60} powder compacted under pressure of 1 GPa ("high-pressure samples") by different processes.[4] Despite the description given by the authors, thermal conductivity does not exhibit a characteristic amorphous behavior: there is no well-defined plateau around 5–10 K, but rather at 50–100 K with a jump at 100 K for one sample. In comparison to previous results,[3] a very interesting point is that a strictly linear regime is observed for both high-pressure samples (HSP) above 100 K. In Ref. 3 the question was raised about the possible existence

of a plateau at lower temperature, expected for amorphous systems, since the linear regime observed on a more or less broad temperature range above the plateau can also be considered as a characteristic of these materials. In order to verify this hypothesis and the universal existence of linear behavior of thermal conductivity in this kind of material, we have performed a measurement of thermal conductivity in a wide temperature range, from 90 mK to 300 K, together with ultrasonic investigations in the frequency range 2–100 MHz, and structural investigations over different scales (mm, μm, and nm) on a sample obtained by a similar way as described in Ref. 1. Another purpose was whether the "phonon-fracton hopping" model,[5,6] based on the strong localization of lattice vibrations in a disordered structure, could account for the data.

Our main results, which are successively developed in different paragraphs, are the following.

(i) The structure is strongly inhomogeneous, mainly amorphous, or disordered on a very small scale, with some minor crystalline inclusions of several tens of nanometers. It shows a fractal-like character on scales between 1 and 100 μm.

(ii) The sound velocity decreases linearly with increasing temperature from 4 to 100 K. The ultrasonic attenuation is strongly frequency (f) dependent, showing simultaneously a Rayleigh-like scattering regime up to 110 MHz, increasing as
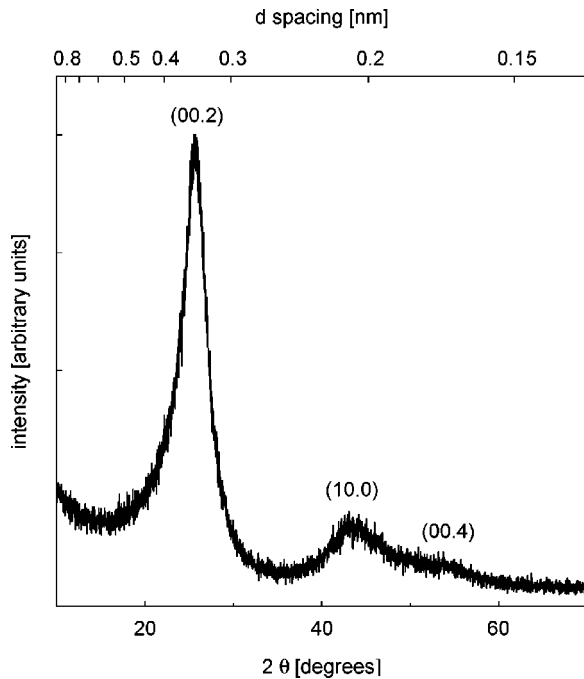
FIG. 1. X-ray diffraction (XRD) pattern of the hard carbon sample prepared under a pressure of 3 GPa and temperature of 973 K for 2 h. The indices are those of graphite. The scale on the top is the d spacing for the mean interatomic distance, for comparison with previous neutron diffraction measurements.

f^3, and a resonant regime peaked at $f = 28$ MHz, corresponding to a scatterer diameter of 70 μm.

(iii) The thermal conductivity is strictly linear in T from 20 to 300 K, which confirms previous experiments.[3] This linear regime can be related to the linear decrease of the sound velocity, according to the ''phonon-assisted fracton hopping'' model of Nakayama and Orbach, established for amorphous stuctures.[6] This corresponds to a structural coherence length (density fluctuations) of 0.5–0.6 nm. Below $T = 10$ K, the thermal conductivity varies as $T^{1.4}$ and is lower than for vitreous silica by a factor of ≈ 5–10, and without the characteristic *plateau* at a few kelvin of amorphous materials. There is appearance of a boundary scattering regime around 100 mK, which corresponds to a scatters size of approximately 45–60 μm.

(iv) Hard carbon is an interesting physical system for studying the localization of acoustic phonons, due to scattering on structural disorder. The large structural disorder of hard carbon shortens the phonon mean free path via Rayleigh scattering. The vibrational excitations cross over from phonon like to fracton like at frequency $f > f_c$, where the critical frequency (f_c) is evaluated to be about 1000 MHz from ultrasonic measurements. This value is three orders of magnitude smaller than that of 440 GHz,[7] determined in vitreous silica.

Since the fractons are spatially localized vibrations, they cannot contribute to the heat transport. The thermal conductivity of hard carbon does not show a ''plateau'' regime, associated with localization of lattice vibrations, in the temperature range 0.1–300 K. The question then arises: how can the spatially localized fractons contribute to the thermal conductivity?

II. SAMPLES

The samples of hard carbon were obtained from C_{60} fullerene, in the form of bulk specimens, at Osaka National Research Institute.[2,8] The initial sample of 99.9% purity C_{60} was treated under a nonhydrostatic pressure of 3 GPa and a temperature of 973 K during 2 h, as described in Ref. 1. The obtained samples of hard carbon are quite homogeneous (i.e., without voids and pores) and have a black color. Their density, 2.06 g/cm³, is slightly larger than the density, 1.9 g/cm³, of hard carbon samples (HC1) prepared previously under similar conditions.[1] The density of hard carbon is larger than that of the initial C_{60} (1.7 g/cm³), but significantly smaller than the density of diamond (3.5 g/cm³), and lies within the boundaries for amorphous carbon (1.8–2.1 g/cm³).[9] Vickers hardness tests reveal that this material is approximately two-thirds as hard as diamond, but the samples did not reveal distinct evidence of crystalline diamond. However, the resistivity measurements show that the material is semimetallic, very similar to graphite.[10] This form of carbon has a hardness that is a substantial fraction of the hardness of diamond, but is still electrically conductive. Neutron diffraction measurements[2] show lack of long-range crystalline order. Due to the large hardness and disordered structure, we have performed the microscopic characterization, acoustic, electrical, and thermal conductivity measurements on specimens of hard carbon prepared under identical conditions.

III. STRUCTURAL INVESTIGATIONS

Although a considerable amount of structural research on similar carbon materials has already been performed (for example, see Refs. 1, 2, and 11–13), their detailed structure is still unknown. The most probable reasons are the closeness of the phase-transition border of several C_{60} phases in this P-T region,[7,11] the instability of the structure in time, and the fact that the structure of different specimens strongly depends on the details of the reaction conditions. Because of that, we emphasize the importance of the structure analysis of the specific sample used at the same time for acoustic and transport measurements. Hereafter we present the structure analysis of the hard carbon sample obtained by several techniques: x-ray diffraction (XRD), transmission electron microscopy (TEM), scanning electron microscopy (SEM), and acoustic scanning microscopy. In addition, an investigation on the micrometer scale has recently started in the E.S.R.F. laboratories in Grenoble. The analysis indicates a very inhomogeneous and disordered structural character on very different scales.

The XRD spectrum was obtained with a Philips PW 1402 automatic diffractometer [λ(Cu$K\alpha$)=0.154 nm]. Three broad peaks are measured at 2θ values of approximately 25.8°, 43.7°, and 51.7° (Fig. 1.) These peaks correspond to d spacing of 0.349, 0.207, and 0.173 nm, respectively. They are similar to the (00.2), (10.0), and (00.4) reflections of graphite (0.338, 0.214, and 0.168 nm, respectively: see Table I), but a diffuse character of the peaks indicates a *non-ordered*

TABLE I. X-ray diffraction data for diamond, graphite (Ref. 13), and hard carbon.

Material	d_{hkl} (nm)		
Diamond	$d_{111}=0.206$	$d_{220}=0.126$	$d_{311}=0.108$
Graphite	$d_{002}=0.338$	$d_{100}=0.214$	$d_{004}=0.168$
		$d_{101}=0.204$	
Hard carbon	$d_{002}=0.349$	$d_{100/101}=0.207$	$d_{004}=0.173$

structure. The more pronounced (00.2) reflection suggests a higher degree of ordering in the c planes. The mean interatomic distance is higher than for either ideal (0.335 nm) or turbostratic (0.344 nm) graphite.[13] Even larger distances are measured on a selected area by electron diffraction: diffuse rings correspond to values of 0.357, 0.211, and 0.175 nm (this difference is due to a local character of the electron diffraction technique, while XRD is an average measurement over the whole sample). As previously pointed out,[1] no peak related to the initial C_{60} (or diamond either) is observed. The XRD and electron diffraction measurements are in agreement with previous neutron diffraction[2] and XRD measurements obtained on samples prepared under similar conditions. In addition, inelastic neutron scattering[2] shows that the density of states does not have any similarity to C_{60} or its orthorhombic phases. This is also confirmed by micro-Raman spectra,[1] which are interpreted as due to nanocrystalline or highly disordered graphite.

The TEM sample preparation consisted of tripod polishing and ion beam thinning in a Gatan Duo Mill at a liquid nitrogen temperature. Images of the sample were made by using a Philips CM 20 and a Hitachi HF-2000 transmission electron microscope. The hard carbon sample appears very inhomogeneous. Although in many parts of the sample no ordered structure can be observed, some parts have a layered structure [Fig. 2(a)], which is probably an effect of the uniaxial pressure applied during the synthesis. Uniaxial ordering is marked on the electron diffraction pattern, producing an intensive reflection spot on a diffuse (00.2) reflection ring [inset of Fig. 2(a)]. High-resolution TEM [Fig. 2(b)] revealed regions with a medium-range ordering on the nanometer scale.

SEM images were performed with a JEOL 840-A microscope on natural surfaces of the samples. They reveal a very disordered structure on scales between 1 and 100 μm with a fractal-like (self-similarity) character (Fig. 3) as a broad distribution of domain sizes in this range. This character is confirmed by other scans on a smaller (2 μm) scale. Sparse areas show layered structures (Fig. 4).

Scanning acoustic microscopy also provides structural information on materials.[14] Since the ultrasonic waves completely penetrate the hard carbon sample, it is possible to image the internal structure. Scanning acoustic microscopy in the pulse echo mode scans a focused acoustic beam over the plane of the sample. The amplitude of the reflected subsurface echo is used to create an image of the internal structure. A commercial (HC 1000 Sonix) acoustic microscope has been used with an ultrasonic pulse generated with a center frequency of 75 MHz. The resolution was 100 μm in
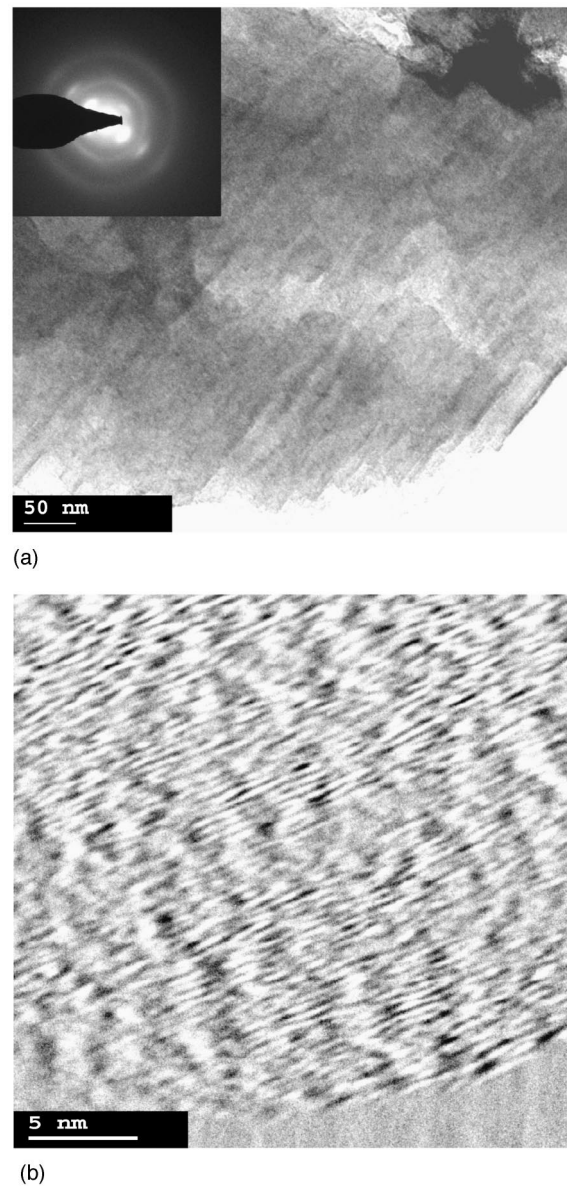

(a)

(b)

FIG. 2. (a) Bright-field TEM micrograph showing the layered structure of the hard carbon. The inset shows the corresponding selected area electron diffraction pattern with three diffuse rings having $d=0.357$ nm, 0.211 nm, and 0.175 nm, in accordance with XRD data. (b) High-resolution TEM micrograph showing a medium-range ordering of the hard carbon in the nanometer scale.

water. The acoustic image of a polished cylinder, diameter of 4.5 mm and length 2.5 mm, of hard carbon shows relative change in amplitude of about 20%, which is assigned to the different elastic properties which are explored locally, which also indicates an (acoustical) inhomogeneity over the submillimetric scale. Careful sample polishing was necessary in order to suppress the contrast coming from the sample surface. Regularly distributed inhomogeneities have also been detected with this technique, as a layered structure of an average thickness of 80 ± 20 μm, oriented perpendicular to the cylinder axis, which is also the direction of the nonhydrostatic applied pressure.

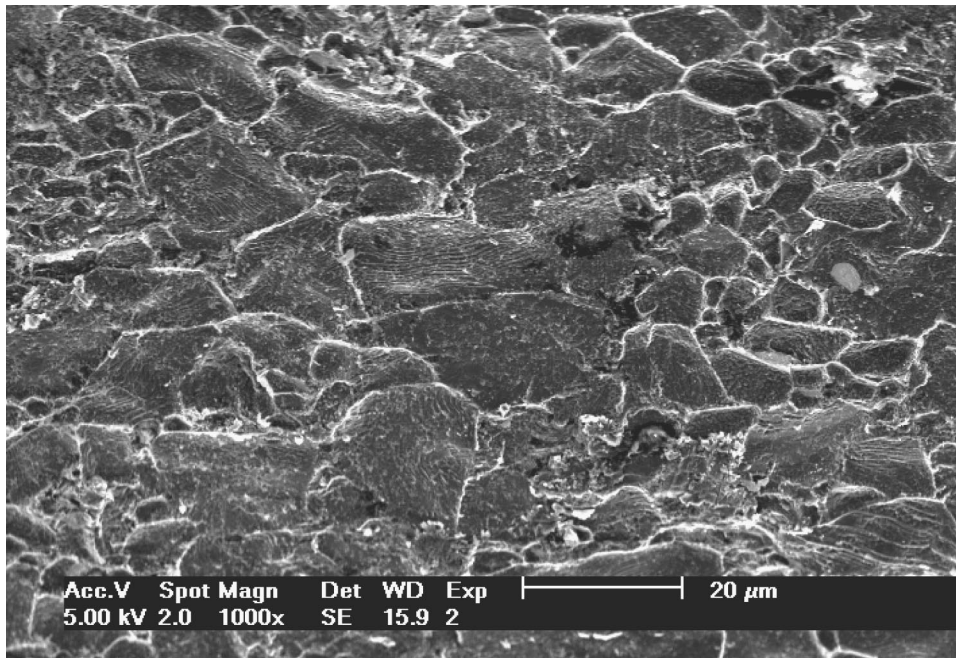Finally, with the exception of the scarce layered structure

FIG. 3. SEM images showing a very inhomogeneous structure on the micrometer scale. SEM reveals sparse areas with organized layered structure on the scale of several micrometers, in accordance with the ultrasonic attenuation data that indicated a broad distribution of phonon scatters size over 8–100 μm.

areas (Figs. 2 and 4), the structure shows an overall self-similarity for scales between ≈ 1 μm and submillimeter.

The larger interatomic distances and lower density of hard carbon compared to graphite, together with an extreme hardness (which is attributed as being a remainder of randomly distributed sp^3 bonds originating from the collapsed C_{60} cages) puts this material forward as a new form of carbon.[11]
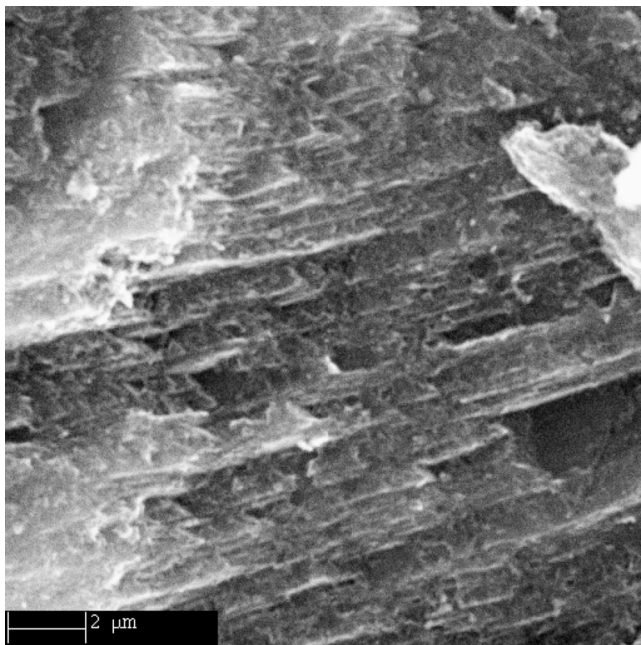

FIG. 4. SEM reveals sparse areas with organized layered structure on a several micrometer scale.

IV. ACOUSTICAL MEASUREMENTS

A. Experiment

Longitudinal and shear waves of the frequencies f in the range of 2–100 MHz were generated as tone-burst pulses resonant and broadband flat transducers.

A sample of hard carbon in the shape of cylinder (diameter of 4.5 mm and length of 8 mm) was used for ultrasonic measurements at low frequencies ($f < 40$ MHz), at room temperature. The variation in the velocity of sound, $\Delta V/V$, at low temperatures was measured by phase-coherent detection, at frequency $f = 15$ MHz.

This sample of hard carbon was used first for the low-temperature thermal conductivity measurements. Then it was polished flat and parallel, the length being reduced to 2.5 mm, for ultrasonic measurements at high frequencies ($f > 40$ MHz). The ultrasonic pulses were fed into the thin sample (length of 2.5 mm) via buffer rods. In order to eliminate the influence of possible nonlinearities on the rf receiver, a balanced technique was adopted to maintain a constant receiver input. The intensity of the ultrasonic waves was varied by 50 dB. The diffraction effects, which are important at low frequencies, have been corrected. A sample of vitreous silica, in the shape of a cylinder with diameter 3 mm and length 10 mm, was measured in the same manner.

B. Results

1. Room temperature

a. Elastic moduli. Elastic moduli have been deduced from the velocities V_L and V_T of longitudinal and shear waves. The longitudinal and shear moduli C_L and G were calculated from the sound velocities according to the well-known relations

$$C_L = \rho V_L^2, \quad G = \rho V_T^2, \tag{1}$$

TABLE II. Calculated density ρ, sound velocities in the longitudinal V_L and transversal V_T directions, the bulk modulus B, shear modulus G, and Poisson ratio σ, calculated from Eqs. (1) and (2) with the coefficient β for hard carbon (HC2 sample) and vitreous silica (Ref. 17).

Material	ρ (g/cm^3)	V_l (m/s)	V_T (m/s)	B (GPa)	G (GPa)	σ	$\beta \times 10^4$ (K^{-1})
Hard carbon	2.06	5900	3400	40	24	0.24	0.29
Vitreous silica	2.20	5800	3800	31.6	31.8	0.12	3.2

where ρ is the density. Other moduli, i.e., the bulk modulus B, Poisson's ratio ν, and Young's modulus E, were obtained from the relations between the elastic moduli of an isotropic medium:

$$B = \rho\left[V_L^2 - \frac{4}{3}V_T^2\right], \quad \nu = \left[1 - 2\frac{V_T^2}{V_L^2}\right] \bigg/ \left[2 - 2\frac{V_T^2}{V_L^2}\right],$$

$$E = G\left[3 - 4\frac{V_T^2}{V_L^2}\right] \bigg/ \left[1 - \frac{V_T^2}{V_L^2}\right]. \tag{2}$$

The values of the elastic moduli calculated from Eqs. (1) and (2) for hard carbon and vitreous silica are given in Table II.

b. Ultrasonic attenuation. Figure 5 shows the frequency-dependent longitudinal attenuation $\alpha(f)$ measured in hard carbon and vitreous silica at room temperature in the frequency range 2–110 MHz. Attenuation is much larger (by one or two orders of magnitude) in hard carbon than that in vitreous silica. Two different behaviors are observed in the frequency dependence of the attenuation, $\alpha(f)$ at low and high frequencies (Figs. 5 and 6). At high frequencies $f > 50$ MHz, the attenuation $\alpha(f)$ is proportional to the third power of the frequency and can be described by the relation

$$\alpha_{\text{high}} = 2.2 \times 10^{-5} f^3, \tag{3}$$

where α_{high} and f are expressed in dB/mm and MHz, respectively. At low frequencies $f < 50$ MHz, the attenuation data $\alpha(f)$ do not follow the power-law dependence (3). A clear change of slope at $f = 28$ MHz is seen in Fig. 6. The attenuation α is analyzed in terms of the equation

$$\alpha = \alpha_{\text{low}} + \alpha_{\text{high}}, \tag{4}$$

where α_{low} is the contribution to the attenuation associated to the low frequencies. α_{low} deduced from the experimental data using Eq. (4) is reported in the inset of Fig. 6. The sharp maximum of α_{low}, at $f_0 = \omega_0/2\pi = 28$ MHz, cannot be described by a relaxation process as

$$\frac{\text{attenuation}}{\text{attenuation}_{\text{max}}} = \frac{2\omega^2/\omega_0}{1 + (\omega/\omega_0)^2},$$

but α_{low} should be associated with a resonant scattering. It is well known that scattering of the ultrasonic waves by identical scatterers (spherical scatterer of radius R) contained in a material gives sharp maxima in the frequency dependence of the attenuation.[15] The first maximum occurs at a wavelength λ, comparable to the size of the inhomogeneities, $kR = 1$,
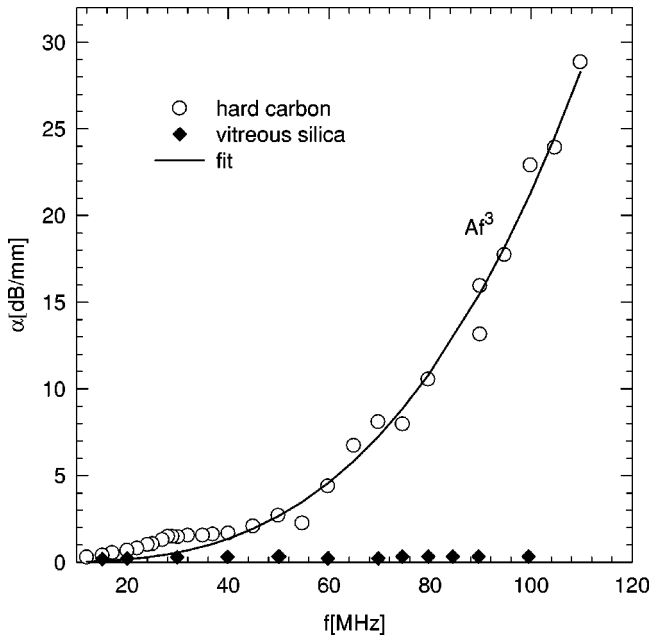

FIG. 5. Frequency dependence of the attenuation, $\alpha(f)$, of longitudinal waves. The solid line is calculated attenuation by using the equation $\alpha_{\text{high}} = 2.2 \times 10^{-5} f^3$ (f is expressed in MHz). Data for vitreous silica ($\blacklozenge$) are shown for comparison.
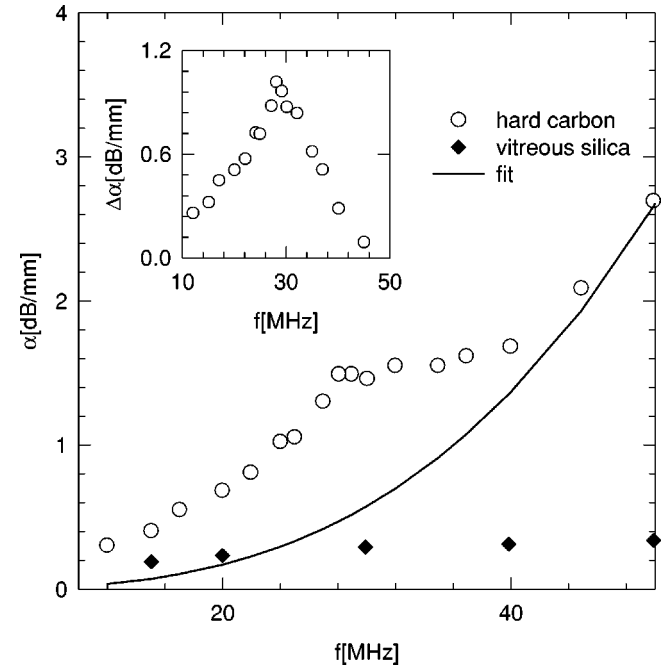

FIG. 6. Frequency dependence of the attenuation, $\alpha(f)$, of longitudinal waves. Inset: the contribution α_{low} deduced from Eq. (4).
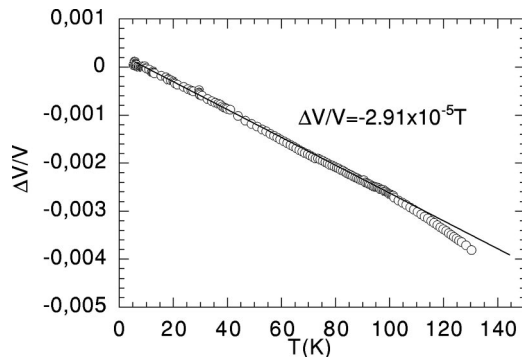
FIG. 7. Temperature dependence of the relative longitudinal velocity change $\Delta V/V(T)$ of hard carbon measured at frequency $f = 15$ MHz.

where k is the wave vector ($k = 2\pi/\lambda$). At frequency $f_0 = 28$ MHz, the ultrasonic wavelength is 210 μm, which gives a radius $R = 35$ μm.

The ultrasonic attenuation α is inversely proportional to the elastic mean free path Λ; for an ultrasonic wave propagating in the x direction, the intensity I falls off as $I = I_0 \exp(-\alpha x)$ or $I = I_0 \exp(-x/\Lambda)$. Extrapolation of Eq. (3) gives $\alpha \approx 600$ dB/mm at a frequency of 300 MHz, and the elastic mean free path is $\Lambda = 15$ μm, which is smaller than the corresponding wavelength $\lambda = 20$ μm at 300 MHz. Within the Ioffe-Regel criterion for localization, $\Lambda < \lambda$, the phonon localization is achieved at frequency above 300 MHz. Assuming a quadratic frequency increase of the attenuation in the frequency range above 100 MHz, a slightly higher critical frequency of 1000 MHz is evaluated: the corresponding mean free path of 4 μm is smaller than the wavelength $\lambda = 6$ μm.

2. Low temperatures

The temperature dependence of the relative velocity change of longitudinal waves is shown in Fig. 7. From the lowest temperatures to about 100 K the velocity decreases linearly with increasing temperature with a slope of $\beta = 2.9 \times 10^{-5}$ K^{-1}. The linear temperature dependence of the velocity at intermediate temperatures is a universal property of amorphous and disordered solids.[16,17]

C. Discussion

1. Ultrasonic attenuation at high frequencies

The scattering of ultrasonic waves by a broad distribution of obstacles has been studied intensively and in particular in polycrystalline materials.[18,19] Scattering by grains contributes to a large part of the ultrasonic attenuation of polycrystalline metals. Rayleigh scattering giving ultrasonic attenuation equal to[19] $\alpha = SWf^4$ (S, W, and f are the Rayleigh scattering factor, the average scattering volume, and the frequency, respectively), occurs when $\lambda > 2\pi D$ (λ is the wavelength and D is the average scatterer diameter). A broad distribution of scatterers exists in hard carbon, as confirmed by spectroscopy measurements.

The frequency dependence of the attenuation often appears to be less than the fourth power, even though Rayleigh scattering is occurring; more often, it is around the third power, other effects being contributing terms which lower the exponent in the attenuation.[19] Thus the Rayleigh scattering behavior permits us to estimate an average size of the scatterers. The wavelength is about 50 μm at a frequency of 100 MHz, which gives an average size of scatterers much smaller than 8 μm. If one asserts the existence of the f^3 regime down to 28 MHz, this yields a distribution of sizes between 8 μm (for $f = 100$ MHz) and 30 μm ($f = 25$–30 MHz), which is in the range of SEM images: a broad distribution of the size of the scatterers exists in the micrometer region as confirmed by the Rayleigh behavior. In contrast, homogeneous vitreous silica gives a small attenuation around 100 MHz (see Fig. 5).

For high frequency $f > f_C$, the mean ultrasonic free path is less than the ultrasonic wavelength, indicating the breakdown of wave propagation. The value of the critical frequency f_C (300 or 1000 MHz) characterizing localization in hard carbon cannot be determined with accuracy from the ultrasonic measurements, but its value is three orders of magnitude smaller than that determined in vitreous silica.[7] This is in marked contrast with amorphous silica where the localization effect has been observed at a very high frequency of about 440 GHz, corresponding to a wavelength of 13.4 nm, and where a mean free path of 10.0 nm has been evaluated by picosecond ultrasonic measurements.[7]

A fractal solid is characterized by a correlation length Ξ, beyond which the solid is homogeneous.[20] As the acoustical vibration frequency is continuously increased, one reaches a crossover frequency f_C where $q\Xi \approx 1$ (q is the wave vector). At this point one expects that the wave becomes strongly scattered: $q\Lambda \approx 1$ (Ref. 21). The exact value of the acoustical correlation length Ξ cannot be given for hard carbon, but a crossover frequency f_C of 300–1000 MHz suggests that $\Xi \approx 1$–10 μm. The latter value is two orders of magnitude larger than the value of $\Xi \approx 100$ nm found in silica aerogels where a similar critical frequency of ≈ 1000 MHz has been found;[22] however, a small sound velocity of 100 m/s is observed in silica aerogels.

2. Resonant attenuation at a frequency of 28 MHz

The resonant contribution to the attenuation around 30 MHz is 3 times larger than that of the Rayleigh contribution. Identical scatterers having mesoscopic size (radius of 35 μm) contribute to these phenomena. Ultrasonic measurements cannot give information on the microscopic nature of these scatterers, but they could be associated with modulations of the mass density or the elastic modulus having the same size of about 35 μm (or diameter of 70 μm). Such a value must be compared with that of 45–60 μm deduced from the thermal measurements at very low temperatures, due to a boundary scattering effect originating from large fluctuations of the elastic constants on this scale.

In conclusion, a broad distribution of scatterers having a size smaller than the wavelength, $D \ll \lambda/2\pi$, is at the origin of the Rayleigh scattering behavior, with the characteristic f^3 variation at $f > 50$ MHz. This regime yields the localization
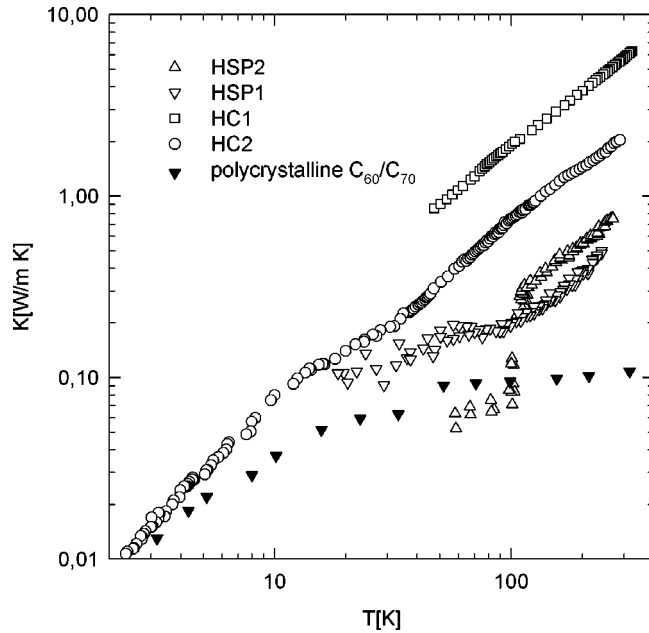
FIG. 8. Comparative plot illustrating the thermal conductivity $\kappa(T)$ for different fullerite samples: hard carbon [HC1 ($\square$): see text] (Ref. 3), high-pressure sample (HSP) made by first applying high pressure and then the high temperature HSP1 (Ref. 4) ($\triangledown$), high-pressure sample made by heating the sample up to a high temperature then applying high pressure HSP2 (Ref. 4) ($\triangle$), and present data of hard carbon [HC2 ($\bigcirc$)]. Also are reported microcrystalline compacted C_{60}/C_{70} data ($\blacktriangledown$, Ref. 23)

of the acoustic waves for frequency $\sim$300–1000 MHz. In addition, identical defects characterized by a large size of 35–70 μm, which give a resonant scattering behavior, are determined at low frequency.

A different behavior is observed in vitreous silica: a very small ultrasonic attenuation is measured in the 10–100 MHz range, which confirms that this material is homogeneous on the micrometer scale.

V. THERMAL CONDUCTIVITY

A. Experiment

The low-temperature (from 90 mK to 6 K) thermal conductivity $\kappa(T)$ was measured in a dilution refrigerator by a conventional steady-state heat-flow technique with one heater and two thermometers, the flow propagating along the pressure axis of the sample. The sample was in the shape of a cylinder of diameter 4.5 mm and total length of 8 mm. Silver paste was used as conducting cement to fix the thermometers and heater on the sample, and also to fix the sample mechanically on the copper substrate acting as the thermal sink. At each temperature, we have measured thermal gradients obtained with various applied powers. We corrected the measured thermal gradient under forced heat flux at each point from the value with null power, which yields a sizable correction for $T \lesssim 200$ mK. We have systematically verified the linearity of the resulting gradient with power. The gradient is about 0.5%–1.5% of T for temperatures above 0.5 K and reaches about 10% of T at the minimum

temperature below 100 mK. In the high-temperature range (4–320 K) a steady-state comparative method relative to a constantan foil was used in a ^{4}He cryostat. The initial sample of hard carbon was cut in a form of prism of length 5.4 mm and triangular cross section of $\approx$2.06 mm^2. The sample was attached with GE varnish to the reference sample, which was also used as a thermal link between the sample and heater. On the other side, the sample was glued directly to a thermal sink. The sample chamber was maintained in vacuum better than 10^{-4} Pa. The heat flow was estimated from the voltage difference between two Chromel wires (diameter of 15 μm) point soldered to the Constantan foil, so that the link was also used as a thermocouple element. The thermal gradient in the sample was measured by a thin Chromel-Constantan thermocouple (diameter of 15 μm) glued to the sample with GE varnish. The temperature difference measured on the sample was always smaller than 1 K. In order to minimize radiation heat losses, the sample holder was closely surrounded by a heat shield kept at almost the same temperature. The cooling (heating) rate was generally $\sim$5 K/h or less. The relative accuracy of the measurement (1%–2%) was much better than for absolute values (about 20%, due to uncertainty in geometrical factors of the sample and the reference). Electrical resistivity was measured independently on the same sample by a conventional four-probe method. Contacts were made using conducting silver paste directly on the surface of the sample.

B. Results and analysis

Figure 8 shows a comparative plot illustrating the evolution of the thermal conductivity $\kappa(T)$ for different fullerite samples with the effect of increase of pressurization on pristine C_{60}. The lower data are for microcrystalline C_{60}/C_{70} (with $\sim$85% C_{60}) obtained by pressurization of 0.3 GPa, with a low density of 1.54 g/cm^3 (Ref. 23). In such samples, Debye-like vibrations play only a role below $\sim$4 K. A remarkable behavior is the saturation to $\kappa \sim 0.1$ W/mK above $T = 40$ K: this value is 10 times smaller than vitreous silica at 300 K and is interpreted within the Einstein model of heat transport by localized oscillators, assumed to vibrate with a random phase.

On increasing pressurization to 1 GPa, two "high-pressure samples" HSP obtained in different ways were measured: HSP1,[4] made by first applying high pressure and then high temperature, and HSP2,[4] a high-pressure sample made by heating the sample up to high temperature, then applying high pressure (however, no detailed structural investigation is given for these samples), and our data for hard carbon (HC2) made under similar conditions (pressure around 3 GPa) as HC1. A very interesting point is the appearance of a strictly linear-in-T regime at high temperature, characteristic of amorphous materials, and its progressive temperature extension upon higher pressurization: down to 20 or 40 K for HC2 and HC1, respectively, compared to only 100 K for HSP samples. Simultaneously, the absolute value of κ increases.

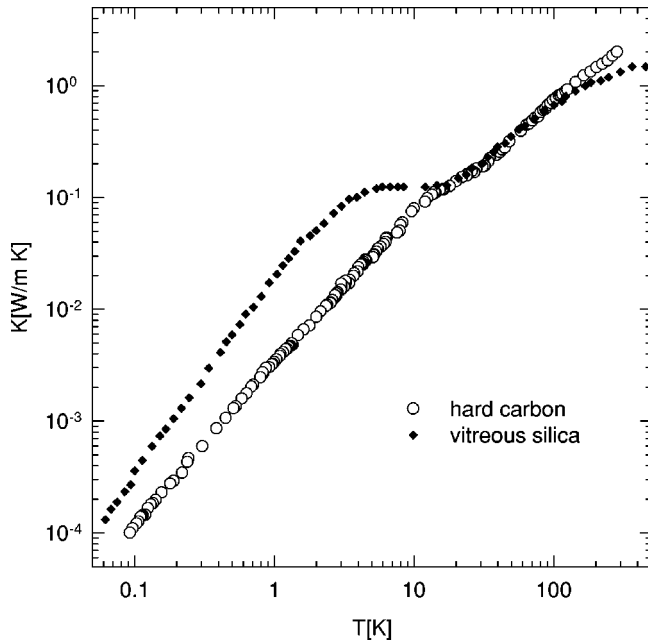Figure 9 presents the thermal conductivity of hard carbon (HC2) in the whole temperature range (from 90 mK to 320

FIG. 9. Thermal conductivity, $\kappa(T)$, of hard carbon (HC2) and vitreous silica (v-SiO$_2$) (Refs. 24 and 25) for comparison.

K) in comparison with the data for vitreous silica (v-SiO$_2$).[24,25] The most intriguing fact is the absence of the *plateaulike* behavior around 5–10 K, which was expected to exist in earlier work,[3] and the lack of T^2 behavior below 1 K as in amorphous material.[24] Only an inflection point, as reminiscent of the end of plateau of v-SiO$_2$, separates a low-T power-law regime ($\propto T^{1.4}$) and the high-T linear regime. This linear behavior at high temperature is present in a wider temperature range, in comparison with v-SiO$_2$, and without any indication for a deviation from linearity up to room temperature, in contrast to v-SiO$_2$, which shows a clear saturation above 100 K. We also note the superposition of both data between 20 and 100 K. Also, we point out that the two sets of data for hard carbon (HC2) measured with two thermometers in the low-temperature region ($T<6$ K) and relative to constantan in the high-temperature region ($T>4$ K) agree very well (see also Fig. 10). The thermal conductivity of hard carbon (HC2) at room temperature is about 2 W/mK. This value is higher than values obtained by Efimov and Mezhlov-Deglin for high-pressure samples,[4] but lower than for previously measured sample HC1.[3]

In the general framework of two species of heat carriers (phonons and electrons), the measured thermal conductivity κ_{tot} is considered as the sum of the "phonon" κ_{ph} and the electronic κ_{el} contributions: $\kappa_{tot}=\kappa_{el}+\kappa_{ph}$. At this point κ_{ph} can be extended to any vibrational excitations. The electronic contribution could be estimated by the Wiedemann-Franz law $\kappa_{el}=L_0\sigma T$, where $L_0=2.45\times10^{-8}$ W Ω K^{-2} is the Lorenz number and σ the electrical conductivity. The electrical conductivity of our sample at the room temperature is relatively high, about 2.8×10^5 Ω^{-1} m^{-1}, and cooling down to 2 K increases it only by about 5%.[26] The temperature dependence substantially deviates from the activated regime typical for the usual glassy carbon,[27] and it is in agreement with previously published data, but the absolute value
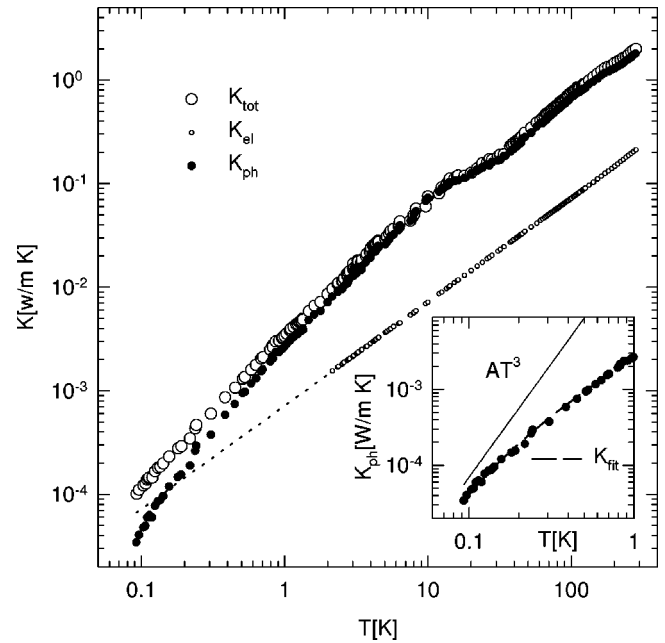

FIG. 10. Temperature dependence of the thermal conductivity κ_{tot} of hard carbon, an estimated electronic contribution to the thermal conductivity, κ_{el}, and the estimated phonon contribution $\kappa_{ph}=\kappa_{tot}-\kappa_{el}$. The inset shows the phonon thermal conductivity κ_{ph} in the low-temperature range ($T<1$ K) in which the boundary effect has been observed. The solid curve through the experimental points was computed from Eq. (5) (see discussion), and the line AT^3, with $A=7.1\times10^{-2}$ (W/mK^4), represents a contribution to the thermal conductivity of boundary scattering.

is several times lower in comparison with previous data.[1] The higher absolute value of electrical conductivity is related to the lower hardness of our sample.[2] The electronic contribution κ_{el}, calculated using the Wiedemann-Franz law and the experimental data of electrical conductivity down to 2 K and the estimated one below 2 K by extrapolation of the higher-T data, is shown on Fig. 10 (open circles and dashed line, respectively), together with the measured thermal conductivity κ_{tot}. The temperature dependence of the electronic contribution κ_{el}, which is linear in T within 5% between 2 and 300 K, is similar to that for the total thermal conductivity and is about 10% of κ_{tot} in the temperature range between 1 and 300 K. Below 1 K, the electronic contribution becomes larger, up to 40%–50% of κ_{tot} at 0.1 K. The deduced "phonon" thermal conductivity $\kappa_{ph}=\kappa_{tot}-\kappa_{el}$ shows a similar behavior as κ_{tot} in the temperature range above 1 K: it shows a linear behavior $\kappa_{ph}(T)\propto T$ from 300 K down to 20 K and a $T^{1.4}$ behavior below 10 K. In the intermediate range κ_{ph} shows the "inflection point." But at the lowest temperature ($T<200$ mK), κ_{ph} starts to deviate from the $T^{1.4}$ law (see the inset of Fig. 10) due to the occurrence of boundary effects.

If one supposes that the low-frequency propagative phonons still contribute up to $T\sim0.2$–0.3 K, we can analyze the vibrational thermal conductivity in the usual way, assuming two different scattering regimes: one being the Casimir boundary scattering due to propagative phonons, the other corresponding to the $T^{1.4}$ law, as

$$\frac{1}{\kappa_{\rm ph}} = \frac{1}{AT^3} + \frac{1}{BT^{1.4}}. \tag{5}$$

Fitting of the data below 1 K yields $A = 7.1 \times 10^{-2}$ (W/mK^4) and $B = 2.8 \times 10^{-3}$ (W/mK$^{2.4}$). The inset of Fig. 10 shows the phonon thermal conductivity $\kappa_{\rm ph}$ in the low-temperature range ($T < 1$ K). The solid curve through the experimental points was computed from Eq. (5), and the line AT^3 represents the limitation of thermal conductivity due to boundary scattering, with $A = 7.1 \times 10^{-2}$ (W/mK^4), which corresponds to the best fit, with the uncertainty due to extrapolation of $\kappa_{\rm el}$ from 2 K, which we estimate to be $6 \times 10^{-2} \leq A \leq 8 \times 10^{-2}$ (W/mK^4). From that value we can estimate the size of the phonon scatterers responsible for this scattering, using the usual kinetic formula $\kappa = (1/3) C_{\rm ph} V_D l$, with l the phonon mean free path (mfp) and $C_{\rm ph}$ the heat capacity of phonons, easily obtained from the sound velocities and density. In the frame of the Debye model,

$$\frac{C_{\rm ph}}{T^3} = \frac{2\pi^2}{5} \frac{k_B^4}{\hbar^3} \frac{1}{\rho V_D^3}, \tag{6}$$

with ρ the density (2.06 g/cm^3) and V_D the Debye mean sound velocity, defined as $3/V_D^3 = 2/V_T^3 + 1/V_L^3$, where V_T and V_L are the transverse and longitudinal sound velocities, respectively. Using the experimental values (see Table II), one obtains $V_D = 3770$ m/s and $C_{\rm ph}/T^3 = 11 \times 10^{-7}$ (J/g K^4). The kinetic formula yields $A = 7.1 \times 10^{-2}$ (W/mK^4) for a phonon mean free path of $l = 51$ μm, within the uncertainty 45 μm $\leq 1 \leq 60$ μm, giving the size of the scatterers. At this point we can note the similarity of this value with that corresponding to the acoustic resonant attenuation (Sec. IV).

C. Discussion

Up to now, we have given a first analysis of the low-T data, assuming the existence of propagating phonons at least to $T \sim 0.2$–0.3 K, at the origin of the boundary scattering regime in good agreement with the size of the scatterers determined by the resonant attenuation at 28 MHz. But on the basis of phonon localization above the crossover frequency of ~ 300–1000 MHz as determined by ultrasonic measurements, one expects that the thermal phonons will be localized on almost the whole T range of the $\kappa(T)$ data. Indeed, within the thermal dominant phonon approximation used in $\kappa(T)$, $\hbar \varpi_{\rm dom} \approx 4.5 k_B T$, thermal phonons generated above $T \sim 10$ mK will be localized. However, a fraction of low-frequency propagating phonons can be acting up to around 10 times this limit,[5,32] i.e., around 100 mK, which could explain the role of boundary scattering in the total scattering process.

We now discuss successively the low-T range ($T \leq 10$ K) characterized by the $T^{1.4}$ power law and the high-T range ($T \geq 20$ K) where $\kappa(T)$ varies linearly with temperature.

The two regimes are separated by an inflection point, which is reminiscent of the upper limit of the plateau of amorphous materials (e.g., vitreous silica).

1. Power law $T^{1.4}$ regime

Within the above hypothesis of phonon localization above a crossover temperature around 10 mK, we suppose this regime to be characteristic of a fractal structure (fractons are localized vibrations) and this result is reminiscent of low-density silica aerogels where a similar power law T^n, with $n = 1.3 \pm 0.1$, was observed *above* 1 K.[28] This hypothesis is supported by the fractal character of this material from the structural observations over the scale from ~ 1 μm to 1 mm. We can try to estimate the power law coefficient n. As proposed by Maynard and co-workers in the frame of a hierarchical model applied to silica aerogels,[28,29] $\kappa \approx T^n$, with $n = \bar{d} + 1 - 2\bar{d}/D$, where D and $\bar{d}$ represent the structural fractal and the spectral dimension, respectively. Using the universal character of critical exponents for percolating systems,[5,20] for the three-dimensional network it is found that $D = 2.5$. Indeed, a similar D value can be used from bulk v-SiO$_2$ to silica aerogels, independently of their density and of the structural details. Furthermore, values $1.1 \leq \bar{d} \leq 1.4$ are obtained for fractal structures of various densities.[5,21,30] For the most studied materials, silica aerogels, different techniques yield $\bar{d} = 1.3 \pm 0.1$ (Ref. 21) or 1.4 ± 0.1 (Ref. 31). From these $\bar{d}$ values and with $D = 2.5$, one gets the power law coefficient $n = 1.26$–1.28. We note that this value is close to the experimental one for silica aerogels (1.3 ± 0.1) and is also in good agreement with the present $n = 1.4$.

In distinction with silica aerogels,[28] we do not observe a plateaulike behavior at very low temperature, which was interpreted as the onset of phonon localization, with a crossover frequency $\varpi_{\rm CO}$ from 0.06 to 0.4 K (Ref. 28). Indeed, in the present case $\varpi_{\rm CO}$ obtained from ultrasonic experiments is a much lower energy. Another striking property is that the thermal conductivity is not so small in comparison to vitreous silica, a homogeneous medium characterized by a much higher frequency of localization of phonons, roughly for $T \approx 5$ K in the plateau regime, corresponding to the frequency of ≈ 450 GHz, a value confirmed by picosecond ultrasonic measurements.[7]

Figure 11 shows, for comparison, the low-temperature ($T < 10$ K) dependence of the thermal conductivity $\kappa/T^{1.4}$ of vitreous silica,[24,25] hard carbon, and "A-NC" aerogel[28] with densities of 2.20, 2.06, and 0.36 g/cm^3, respectively. It should be noticed that at low temperature, the less-dense material exhibits lower thermal conductivity and the thermal conductivity follows the power law behavior $\kappa(T) \approx T^n$ with smaller n. In that T range, the quadratic variation for v-SiO$_2$ is characteristic for resonant scattering of phonons by two-level systems.

2. Linear-in-T regime

The strictly linear-in-T regime has been theoretically proposed by Orbach and co-workers on the basis of "phonon-assisted localized vibrational hopping" processes. Initially, this model was established for fracton-vibrational excitations, assuming some fractal properties of amorphous structures,[5] and it was extended to the more general case of localized excitations, a general property of strongly disor-
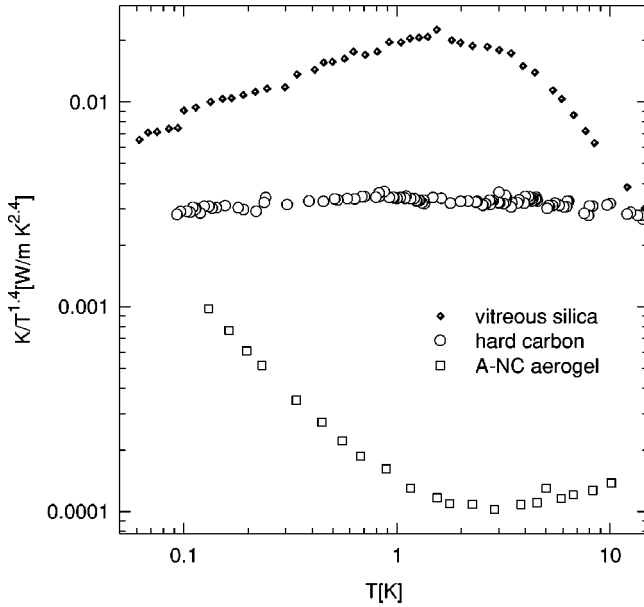
FIG. 11. Low-temperature $(T < 10 \text{ K})$ thermal conductivity $\kappa/T^{1.4}$ vs T of three materials of different densities for comparison: vitreous silica $(v\text{-}SiO_2)$ (Refs. 24 and 25), hard carbon (HC2), and A-NC aerogel (Ref. 28) of densities 2.2 g/cm^3, 2.06 g/cm^3, and 0.36 g/cm^3, respectively.

dered structures.[6,32] Due to localization of phonons above the critical frequency ω_C, which is at the origin of the plateau in $\kappa(T)$ in glasses at $T \approx 10$ K, the hopping process of the localized vibrational excitations assisted by low-frequency phonons (of $\omega \lesssim \omega_C$) adds a linear-in-T contribution to the saturated κ_{ph}. Moreover, this model establishes a direct proportionality between the linear variation of the thermal conductivity and that of the sound velocity in the same T range:[32,33]

$$\frac{\Delta V}{V} = -0.1 \frac{\xi^2}{2\pi^2 V} \frac{\kappa(T)}{T} k_B^{-1} T \qquad (7)$$

(with k_B the Boltzman constant). In this relation, ξ means either the phonon mean free path at the crossover frequency ω_c between extended states $(\omega < \omega_c)$ and localized regime $(\omega > \omega_c)$ where ξ equals the phonon wavelength $\lambda = 2\pi V/\omega_c$ or a mesoscopic structural correlation length,[6,33,34] related to density-density correlations[34] in amorphous materials. For vitreous silica for which the above model was successfully applied, both definitions yield very similar values for $\xi = 1.5$–1.7 nm (1.5 nm from Ref. 33, 1.7 nm from Ref. 34), with a corresponding critical frequency of a few THz. Since both properties, linearity-in-T of $\kappa(T)$ and of the relative variation of the sound velocity, are observed in our case, we have applied the model in order to determine ξ, which is now connected to the amorphous structure of hard carbon on the nanometer scale.

In the present case, the numerical coefficient of the linear variation of $\kappa(T)$ is similar to that of vitreous silica (see Fig. 9), as for the absolute value of the longitudinal sound velocity (see Table II). However, the coefficient of the linear relative variation of the longitudinal sound velocity, $\Delta V/V$

$= -\beta(T - T_0)$, is 10 times smaller than for vitreous silica[16] with $\beta = 2.9 \times 10^{-5}$ K^{-1} in comparison with 3.2×10^{-4} K^{-1} in vitreous silica. From relation (7), it means that the ξ value is about 3 times smaller than for vitreous silica, which is no longer a mesoscopic scale, but a few interatomic distances of ≈ 0.5–0.6 nm, to be compared with the first near-neighbor distances determined from x-ray diffraction: 0.18 nm (very weak signal), 0.21 nm, and 0.35 nm.

A strong discrepancy exists for hard carbon between the two correlation lengths ξ estimated in the nanometer scale using Eq. (7) and Ξ evaluated in the micrometer scale (despite its rough estimation) by the ultrasonic measurements, in contrast with vitreous silica.

VI. CONCLUSIONS

In conclusion, the present acoustical and thermal transport measurements performed on HC samples have revealed several properties characteristic of amorphous or highly disordered polycrystalline structures. The most typical are the following.

(i) a Rayleigh-like regime for ultrasonic attenuation, for frequencies between a few MHz to 110 MHz, which indicates a broad distribution of the phonon scatterers over the tens of micrometers in size, in accordance with the very inhomogeneous structure on this scale shown by the SEM images, at variance with homogeneous glasses like $v\text{-}SiO_2$.

(ii) The dramatic increase in the ultrasonic attenuation with frequency, which gives evidence for a crossover from extended phonon excitations to localized fracton excitations at the critical frequency of about 300 to 1000 MHz; a correlation length Ξ of about 1–10 μm is evaluated.

(iii) In addition to the Rayleigh regime, a resonant acoustic attenuation at $f = 28$ MHz, which corresponds to strong acoustic fluctuations at domains size of about 70 μm (in diameter) exists. This is very probably at the origin of the low-T boundary scattering regime for $\kappa(T)$, where the phonon mean free path is limited to 45–60 μm.

(iv) The linear-in-T variation of the (longitudinal) sound velocity for $T > 4$ K, typical for disordered polycrystalline or aperiodic crystals, which appears to be well correlated with the strictly linear-in-T thermal conductivity in almost the same T range $(T > 20$ K) is observed. Using the "phonon-assisted localized vibrational hopping model" of Orbach, which correlates both properties, one can yield a crossover length ξ (for the phonon localization), which can be identified as the mesoscopic structural correlation length in glasses; here, ξ equals 0.5–0.6 nm. This nanometric-scale correlation is related to the strongly disordered or ill-crystallized structure over a few interatomic distances, which is confirmed by broadening of the x-ray diffraction peaks, as well as by the TEM images of the few crystallites areas. However, there is an unexplained discrepancy between the two correlation lengths, determined by different types of measurements, on different temperature ranges. This is perhaps due to the very inhomogeneous structure of this material.

(v) A very continuous T dependence like $T^{1.4}$ for the vi-

brational thermal conductivity below 10 K. This dependence is similar to that measured above 2 K in low-density fractal silica aerogel, whereas the present amplitude is larger, probably due to the much larger density, and closer to homogeneous vitreous silica. Such an interpretation, based on the localized nature of fracton excitations, agrees with the very small localization frequency indicated above.

(vi) The power-law coefficient (1.4) is in agreement with the fractal and spectral dimension values obtained for very different fractal structures, in particular in silica aerogels of various densities. This interpretation is also supported by the fractal-like structure observed on scales from less than 1 μm to 1 mm. Despite the similarity of $\kappa(T)$ with that of v-SiO_2 above 20 K, the low-T (< 1 K) value is much smaller, which indicates a scattering process very different and much more efficient than phonon scattering by two-level systems, characterized by a T^2 variation.

---

*Corresponding author. FAX: 33-4-76-87 50 60. Electronic address: lasjau@labs.polycnrs-gre.fr

[1] M. E. Kozlov, M. Hirabayshi, K. Nozaki, M. Tokumoto, and H. Ihara, Appl. Phys. Lett. **66**, 1199 (1995).

[2] S. M. Bennington, N. Kitamura, M. G. Cain, M. H. Lewis, and M. Arai, Physica B **263−264**, 632 (1999).

[3] A. Smontara, K. Biljakovic, D. Staresinic, D. Pajic, M. E. Kozlov, M. Hibayashi, M. Tokumoto, and H. Ihara, Physica B **219−220**, 160 (1996).

[4] V. B. Efimov and L. P. Mezhov-Deglin, Physica B **263−264**, 705 (1999).

[5] A. Jagannathan, R. Orbach, and O. Entin-Wohlman, Phys. Rev. B **39**, 13 465 (1989).

[6] T. Nakayama and R. Orbach, Physica B **263−264**, 261 (1999).

[7] H. J. Maris, in *Phonon Scattering in Condensed Matter VII*, Springer Series in Solid State Physics Vol. 112, edited by M. Meissner and R. O. Pohl (Springer-Verlag, Berlin, 1993), p. 256.

[8] R. A. Wood, M. H. Lewis, G. West, S. M. Bennington, M. G. Cain, and N. Kitamura, J. Phys.: Condens. Matter **12**, 10 411 (2000).

[9] J. Robertson, Adv. Phys. **35**, 317 (1986).

[10] K. Matsubara, K. Sugihara, and T. Tsuzuku, Phys. Rev. B **41**, 969 (1990).

[11] V. D. Blank, S. G. Buga, G. A. Dubitsky, N. R. Serebryanaya, M. Yu. Popov, and B. Sundqvist, Carbon **36**, 319 (1998).

[12] L. Marques, J. L. Hodeau, M. Núñez-Regueiro, and M. Perroux, Phys. Rev. B **54**, 12 633 (1996).

[13] M. S. Dresselhaus, G. Dreselhaus, K. Sugihara, I. L. Spain, and H. A. Goldberg, *Graphite Fibbers and Filaments* (Springer-Verlag, Berlin, 1988), p. 44.

[14] For a review, see A. Briggs, in *Advances in Acoustic Microscopy*, edited by A. Briggs (Plenum, New York, 1995).

[15] C. A. Condat, J. Acoust. Soc. Am. **83**, 441 (1988).

[16] B. E. White and R. O. Pohl, Z. Phys. B: Condens. Matter **100**, 401 (1996).

[17] K. A. Topp and D. G. Cahill, Z. Phys. B: Condens. Matter **101**, 235 (1996).

[18] P. C. Waterman and R. Truell, J. Math. Phys. **2**, 512 (1962).

[19] E. P. Papadakis, J. Acoust. Soc. Am. **37**, 703 (1965).

[20] *Fractals and Disordered Systems*, edited by A. Bunde and S. Havlin (Springer-Verlag, Berlin, 1991).

[21] E. Courtens, R. Vacher, and E. Stoll, Physica D **38**, 41 (1989).

[22] E. Courtens, C. Lartigue, F. Mezei, R. Vacher, G. Coddens, M. Foret, J. Pelous, and T. Woignier, Z. Phys. B: Condens. Matter **79**, 1 (1990).

[23] J. R. Olson, K. A. Topp, and R. O. Pohl, Science **259**, 1145 (1993).

[24] R. C. Zeller and R. O. Pohl, Phys. Rev. B **4**, 2029 (1971).

[25] D. G. Cahill and R. O. Pohl, Phys. Rev. B **35**, 4067 (1987).

[26] A. Bilusic, S. Gradecak, A. Tonejc, A. T. Tonejc, J. C. Lasjaunias, and A. Smontara, Synth. Met. **121**, 1121 (2001).

[27] T. Noda, M. Inagaki, and S. Yamada, J. Non-Cryst. Solids **1**, 285 (1969).

[28] A. M. de Goer, R. Calemczuk, B. Salce, J. Bon, E. Bonjour, and R. Maynard, Phys. Rev. B **40**, 8327 (1989).

[29] R. Maynard, Physica A **168**, 469 (1990).

[30] R. Calemczuk, A. M. de Goer, B. Salce, R. Maynard, and A. Zarembowitch, Europhys. Lett. **3**, 1205 (1987).

[31] R. Vacher, E. Courtens, G. Coddens, A. Heidemann, Y. Tsujimi, J. Pelous, and M. Foret, Phys. Rev. Lett. **65**, 1008 (1990).

[32] R. Orbach, Philos. Mag. B **65**, 289 (1992).

[33] A. Jagannathan and R. Orbach, Phys. Rev. B **41**, 3153 (1990).

[34] S. R. Elliott, Europhys. Lett. **19**, 201 (1992).